Cen, Wei; Hoppe, Ralph; Lu, Rongbo; Cai, Zhaoquan; Gu, Ning:

3D highly heterogeneous thermal model of pineal gland in-vitro study for electromagnetic exposure using finite volume method

Original published in:	AIP Advances. - New York, NY : American Inst. of Physics. - 7 (2017), 8, art. 085222, 9 pp.
Original published:	2017-08-25
ISSN:	2158-3226
DOI:	10.1063/1.4991464
[*Visited:*	2019-04-10]

3D highly heterogeneous thermal model of pineal gland in-vitro study for electromagnetic exposure using finite volume method

Wei Cen,[1,2] Ralph Hoppe,[3] Rongbo Lu,[4] Zhaoquan Cai,[5,b] and Ning Gu[6,a]
[1]*Technische Universität Ilmenau, 98684, Germany*
[2]*Nanjing University of Chinese Medicine, 210023, China*
[3]*Ganzheitliches Gesundheits Zentrum, 34305, Germany*
[4]*Jishou University, 416000, China*
[5]*Huizhou University, 516007, China*
[6]*The Third Affiliated Hospital of Nanjing University of Chinese Medicine, 210001, China*

(Received 21 June 2017; accepted 7 August 2017; published online 25 August 2017)

In this paper, the relationship between electromagnetic power absorption and temperature distributions inside highly heterogeneous biological samples was accurately determinated using finite volume method. An in-vitro study on pineal gland that is responsible for physiological activities was for the first time simulated to illustrate effectiveness of the proposed method. [http://dx.doi.org/10.1063/1.4991464]

I. INTRODUCTION

In recent years, wireless telephones have been widely used in our life. There is an increasing public concern about the health hazards resulting from exposure to cell phone radiofrequency (RF) radiation. The International Agency for Research on Cancer (IARC) classified RF radiation as a possible human carcinogen.[1] An interesting finding of the U.S. National Toxicology Program (NTP) support the IARC conclusions regarding the possible carcinogenic potential of RF radiation and reports that "low incidences of tumors in the brains and hearts of male rats, but not in female rats."[2] Temperature elevation from RF energy absorption (usually expressed in terms of the specific absorption rate SAR) is known to be a dominant factor inducing adverse health effects. The difficulty existing in the analysis of the temperature rise in biological bodies caused by electromagnetic fields is the highly complex computation and the lack of preciseness.

The bio-heat transfer equation for homogeneous material model can be easily calculated by using second order finite difference approximation to discretize the spatial derivatives. However, for highly heterogeneous thermal model, the spatial derivative $\nabla(K\cdot\nabla T)$ is difficult to be discretized using FDTD. For a large object, such as human head or human body, the second order finite difference expressions might be suitable enough, but in practice, the in-vitro studies on cells or isolated tiny tissues are often desirable which require accurate simulation. To overcome the disadvantages of the FDTD method, the Finite Volume Method (FVM)[3] has been investigated by researchers. The method is based on integral conservation and therefore has distinct advantages for being readily applicable to multidimensional problems involving variable mesh and physical properties. We propose numerical methods that use FVM method to analyse the fundamental problem of bio-heat transfer caused by electromagnetic (EM) exposure for inhomogeneous materials models. To the best of our knowledge, the method has not been utilized to calculate bio-thermal response of pineal gland caused by electromagnetic exposure. Melatonin which is secreted by the pineal gland in the brain is a major regulator of core

[a]Corresponding author: sonnelichtsonne@gmail.com
[b]Corresponding author: caizhaoquanhz@163.com

body temperature. We recently conducted an in-vitro study on pineal gland that is responsible for physiological activities.

II. METHODS

Biological media are highly heterogeneous, thermal conductivity K varies from tissue to tissue. The bio-heat transfer equation is expressed as:[4]

$$\nabla(K \cdot \nabla T) + A_0 + SAR \cdot \rho - B \cdot (T - T_b) = C_p \cdot \rho \cdot \frac{\partial T}{\partial t} \tag{1}$$

with the boundary condition

$$K\frac{\partial T}{\partial n} = -h \cdot (T - T_a) \tag{2}$$

where K is the thermal conductivity $[J/(s \cdot m \cdot {}^\circ C)]$; A_0 is volumetric heat sources $[J/(s \cdot m^3)]$ due to metabolic processes; the specific absorption rate (SAR) is the input EM heating source into the bio-heat equation; B is a parameter proportional to the blood perfusion $[J/(s \cdot m^3 \cdot {}^\circ C)]$; $T_a$is the ambient temperature; T_b is the blood temperature; h is the convective heat-transfer coefficient $[W/m^2 \cdot {}^\circ C]$; and C_p $[J/(kg \cdot {}^\circ C)]$ and ρ $[kg/m^3]$ are the tissue specific heat and density, respectively.

Many tasks require the in-vitro studies on cells or isolated tiny tissues. If the solution is not sufficiently smooth, the order of accuracy will be reduced. This can happen if the coefficients are not smooth, e.g., due to the thermal conductivity jump across the interface of different tissues. We propose in this context the FVM method which is fully compatible with the FDTD method and allows the use of highly inhomogeneous objects. FVM is developed from integral interpolation method of FD. As the name implies, a finite-volume formulation involves integrating equation over a control volume (CV).

The method has been described previously.[5] Briefly, using the notations in field theory, Eq. (1) can be rewritten as:

$$\frac{\partial T}{\partial t} = div(\nu \cdot gradT) + S \tag{3}$$

where $\nu = \frac{K}{C_p \cdot \rho}$, $S = \frac{A_0 + SAR \cdot \rho - B \cdot (T - T_b)}{C_p \cdot \rho}$.

Integrating Eq. (3) in the control unit $[x_{i-1/2}, x_{i+1/2}] \times [y_{j-1/2}, y_{j+1/2}] \times [z_{k-1/2}, z_{k+1/2}] \times [t_n, t_{n+1}]$ for each CV:

$$\iiint_V \int_{t_n}^{t_{n+1}} \frac{\partial T}{\partial t} dt dx dy dz = \int_{t_n}^{t_{n+1}} \iiint_V div(\nu gradT) dx dy dz dt + \int_{t_n}^{t_{n+1}} \iiint_V S dx dy dz dt \tag{4}$$

The integral on the left-hand side of Eq. (4) can be removed by means of the mean value theorem for integrals. Similarly, the integral over S is removed. The volume integral over the divergence of the heat flux vector is transformed to a surface integral by means of the divergence theorem $\int_V \nabla \cdot (\nu gradT) dV = \int_S (\nu gradT) \cdot \vec{n} dS = \int_S \nu \frac{\partial T}{\partial n} dS$. Eq. (4) can be expressed as:

$$\begin{aligned}
&\frac{\Delta x_{i-1} + \Delta x_i}{2} \cdot \frac{\Delta y_{j-1} + \Delta y_j}{2} \cdot \frac{\Delta z_{k-1} + \Delta z_k}{2} \cdot (T_{ijk}^{n+1} - T_{ijk}^{n}) = \\
&\frac{\Delta y_{j-1} + \Delta y_j}{2} \cdot \frac{\Delta z_{k-1} + \Delta z_k}{2} \cdot \int_{t_n}^{t_{n+1}} \left[(\nu \frac{dT}{dx})_{i+\frac{1}{2},j,k} - (\nu \frac{dT}{dx})_{i-\frac{1}{2},j,k} \right] dt + \\
&\frac{\Delta x_{i-1} + \Delta x_i}{2} \cdot \frac{\Delta z_{k-1} + \Delta z_k}{2} \cdot \int_{t_n}^{t_{n+1}} \left[(\nu \frac{dT}{dy})_{i,j+\frac{1}{2},k} - (\nu \frac{dT}{dy})_{i,j-\frac{1}{2},k} \right] dt + \\
&\frac{\Delta x_{i-1} + \Delta x_i}{2} \cdot \frac{\Delta y_{j-1} + \Delta y_j}{2} \cdot \int_{t_n}^{t_{n+1}} \left[(\nu \frac{dT}{dz})_{i,j,k+\frac{1}{2}} - (\nu \frac{dT}{dz})_{i,j,k-\frac{1}{2}} \right] dt + \\
&\frac{\Delta x_{i-1} + \Delta x_i}{2} \cdot \frac{\Delta y_{j-1} + \Delta y_j}{2} \cdot \frac{\Delta z_{k-1} + \Delta z_k}{2} \cdot \int_{t_n}^{t_{n+1}} \bar{S}_{i,j,k} dt
\end{aligned} \tag{5}$$

Using half-grid central differences, Eq. (5) can be simplified to yield Temperature updating equation:

$$
\begin{aligned}
T_{ijk}^{n+1} = T_{ijk}^{n} &+ \frac{2\cdot\Delta t\cdot \nu_{i-\frac{1}{2},j,k}}{(\Delta x_{i-1}+\Delta x_i)\cdot\Delta x_{i-1}} T_{i-1,j,k}^{n} + \frac{2\cdot\Delta t\cdot \nu_{i+\frac{1}{2},j,k}}{(\Delta x_{i-1}+\Delta x_i)\cdot\Delta x_i} T_{i+1,j,k}^{n} - \\
&\left(\frac{2\cdot\Delta t\cdot \nu_{i-\frac{1}{2},j,k}}{(\Delta x_{i-1}+\Delta x_i)\cdot\Delta x_{i-1}} + \frac{2\cdot\Delta t\cdot \nu_{i+\frac{1}{2},j,k}}{(\Delta x_{i-1}+\Delta x_i)\cdot\Delta x_i}\right) T_{i,j,k}^{n} + \\
&\frac{2\cdot\Delta t\cdot \nu_{i,j-\frac{1}{2},k}}{(\Delta y_{j-1}+\Delta y_j)\cdot\Delta y_{j-1}} T_{i,j-1,k}^{n} + \frac{2\cdot\Delta t\cdot \nu_{i,j+\frac{1}{2},k}}{(\Delta y_{j-1}+\Delta y_j)\cdot\Delta y_j} T_{i,j+1,k}^{n} - \\
&\left(\frac{2\cdot\Delta t\cdot \nu_{i,j-\frac{1}{2},k}}{(\Delta y_{j-1}+\Delta y_j)\cdot\Delta y_{j-1}} + \frac{2\cdot\Delta t\cdot \nu_{i,j+\frac{1}{2},k}}{(\Delta y_{j-1}+\Delta y_j)\cdot\Delta y_j}\right) T_{i,j,k}^{n} + \\
&\frac{2\cdot\Delta t\cdot \nu_{i,j,k-\frac{1}{2}}}{(\Delta z_{k-1}+\Delta z_k)\cdot\Delta z_{k-1}} T_{i,j,k-1}^{n} + \frac{2\cdot\Delta t\cdot \nu_{i,j,k+\frac{1}{2}}}{(\Delta z_{k-1}+\Delta z_k)\cdot\Delta z_k} T_{i,j,k+1}^{n} - \\
&\left(\frac{2\cdot\Delta t\cdot \nu_{i,j,k-\frac{1}{2}}}{(\Delta z_{k-1}+\Delta z_k)\cdot\Delta z_{k-1}} + \frac{2\cdot\Delta t\cdot \nu_{i,j,k+\frac{1}{2}}}{(\Delta z_{k-1}+\Delta z_k)\cdot\Delta z_k}\right) T_{i,j,k}^{n} + \Delta t\cdot \bar{S}_{i,j,k}
\end{aligned}
\tag{6}
$$

In order to ensure the numerical stability, the maximum time step is chosen to satisfy the stability criterion $\delta_t \le \frac{2\rho c_p {\delta_{\min}}^2}{12k+B{\delta_{\min}}^2}$ which was derived from Von Neumann's condition.[6]

By expanding in its finite volume approximation, Eq. (2) can be written as

$$
T_{i_{\min},j,k}^{n+1} = \frac{2K_{i_{\min},j,k}\cdot T_{i_{\min}+1,j,k} - hT_a(\Delta x_{i_{\min}+1}+\Delta x_{i_{\min}})}{2K_{i_{\min},j,k} - h\cdot(\Delta x_{i_{\min}+1}+\Delta x_{i_{\min}})} \tag{7}
$$

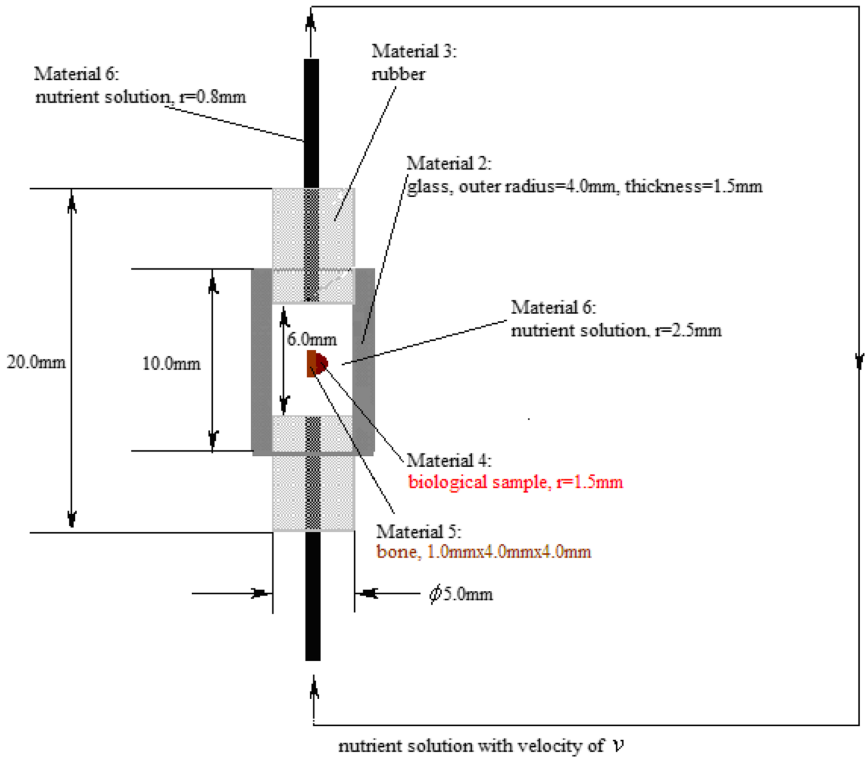

FIG. 1. Central lateral plane of a model for in-vitro studies on pineal gland. Material 1: Air. Material 2: Glass. Material 3: Rubber. Material 4: Pineal gland. Material 5: Attached skull. Material 6: Krebs–Ringer buffer was pumped through the glass cylinder receptacle.

TABLE I. Thermal Properties Assumed for the Various Materials.

Material	$\rho[kg/m^3]$	$C_p[J/kg\cdot^\circ C]$	$K[W/m\cdot^\circ C]$
1	1.3	1017	0.0234
2	2700.0	670	0.6980
3	36.9	3140	0.0420
4	1040.0	3700	0.5700
5	1810.0	1300	0.3000
6	1000.0	4180	0.5500

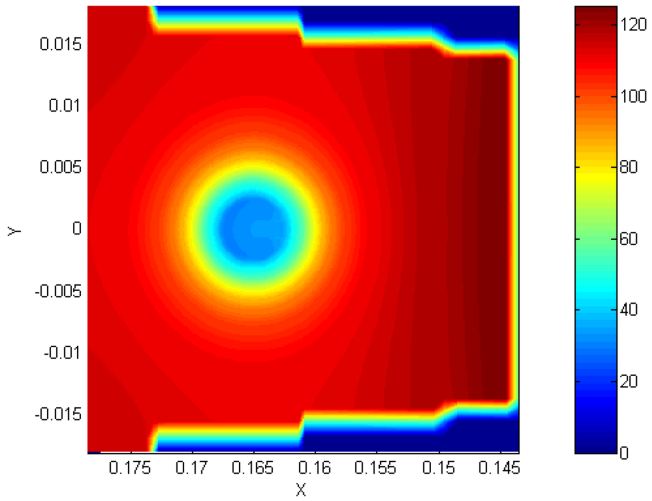

FIG. 2. E-field (magnitude) distribution on the XY observation plane cutting the centre of the pineal gland in-vitro model (frequency = 1800MHz).

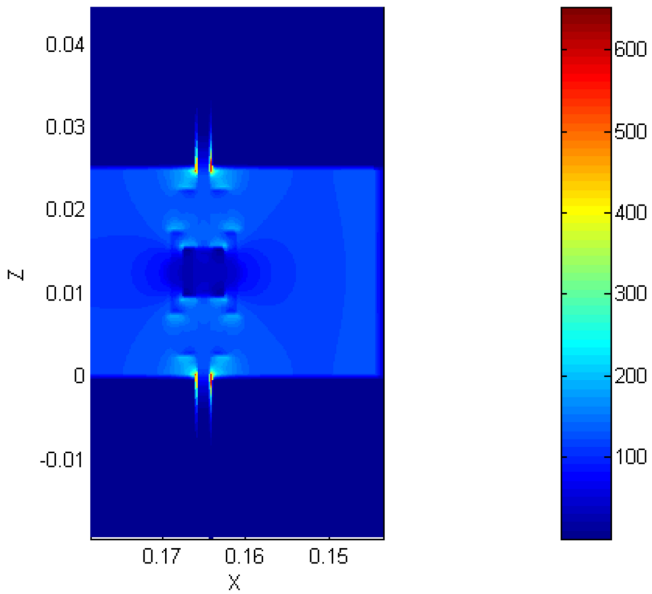

FIG. 3. E-field (magnitude) distribution on the XZ observation plane cutting the centre of the pineal gland in-vitro model (frequency = 1800MHz).

III. NUMERICAL EXAMPLE

Equations (6) and (7) can be easily implemented on a computer. To illustrate effectiveness of the proposed method, the in-vitro study on pineal gland shown in Figure 1 in a sector of the radial waveguide exposure system[7] was conducted.

It is calculated for 6 different materials, including the air surrounding the model, glass, rubber, pineal gland, attached skull, and Krebs–Ringer buffer. Table I lists the thermal properties of all materials.

Figure 2–4 show the electric field distributions plotted across the centre of the model due to excitation of 1800MHz. Determination of the electromagnetic heating source[8] will not be discussed in this paper.

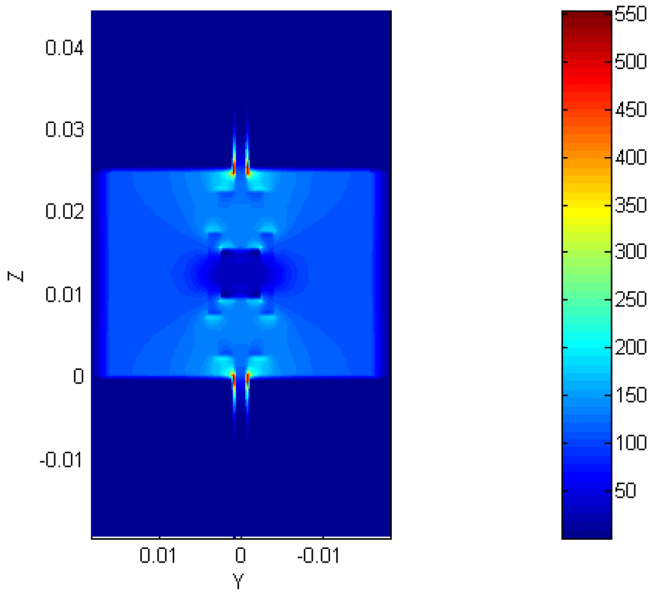

FIG. 4. E-field (magnitude) distribution on the YZ observation plane cutting the centre of the pineal gland in-vitro model (frequency = 1800MHz).

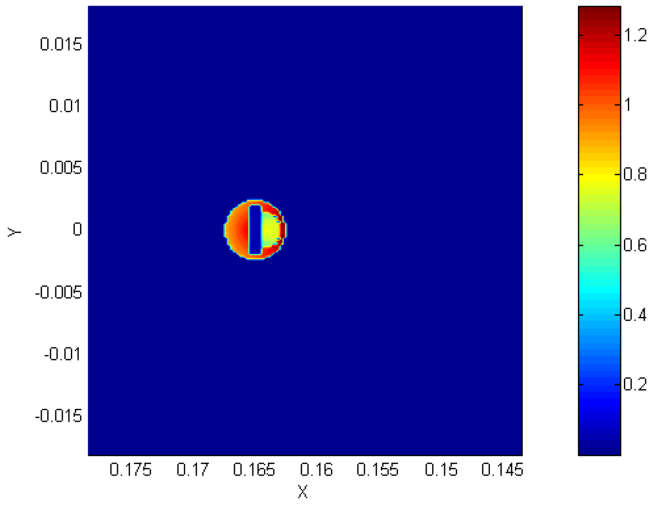

FIG. 5. Specific absorption rate (SAR) distribution inside the pineal gland in-vitro model. The XY observation plane is at the centre of the model. The isolated pineal gland is exposed to a 1800 MHz TEM wave at 0.8 W/kg average SAR.

The specific absorption rate distribution is evaluated as:

$$SAR(i,j,k) = \frac{\sigma(i,j,k)\left[\hat{E}_x{}^2(i,j,k) + \hat{E}_y{}^2(i,j,k) + \hat{E}_z{}^2(i,j,k)\right]}{2\rho(i,j,k)} \tag{8}$$

where $\sigma(i, j, k)$ and $\rho(i, j, k)$ are the conductivity and density of the tissue filling the (i, j, k) cell.

Figure 5–7 show the SAR distributions inside this pineal gland in-vitro model.

The temperature rise of the target model after 5 min exposure was calculated at 800 mW/kg average SAR in the small pineal organ. The initial temperature began from 37°*C*. Figure 8–10 show

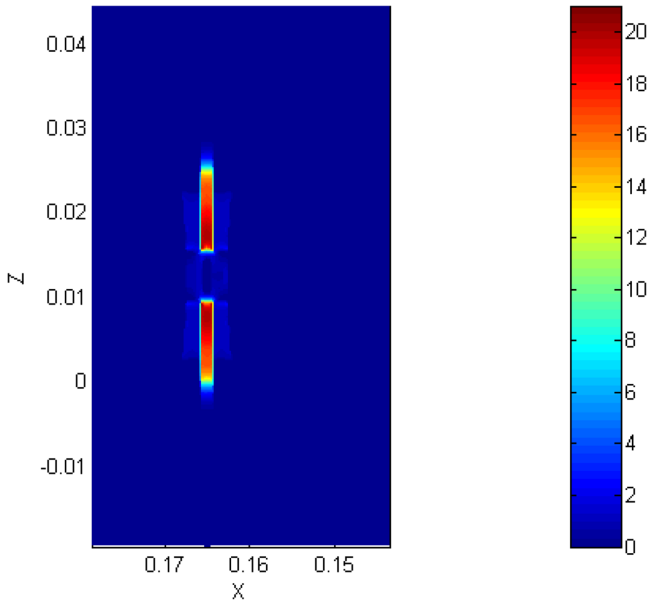

FIG. 6. Specific absorption rate (SAR) distribution inside the pineal gland in-vitro model. The XZ observation plane is at the centre of the model. The isolated pineal gland is exposed to a 1800 MHz TEM wave at 0.8 W/kg average SAR.

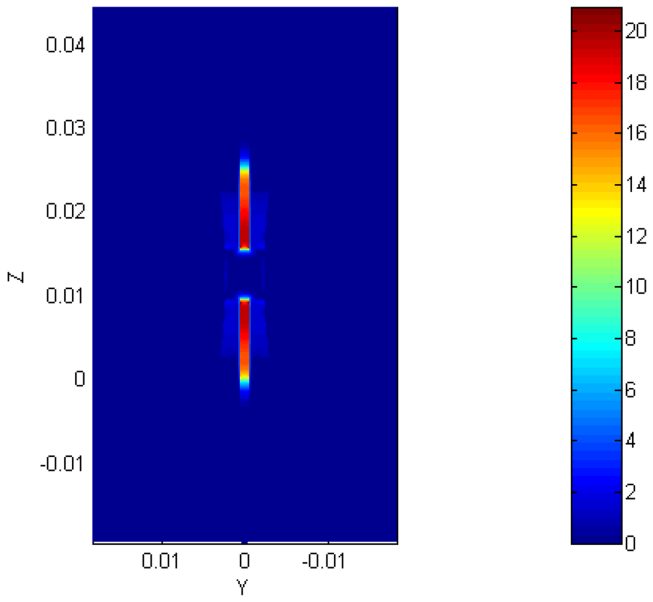

FIG. 7. Specific absorption rate (SAR) distribution inside the pineal gland in-vitro model. The YZ observation plane is at the centre of the model. The isolated pineal gland is exposed to a 1800 MHz TEM wave at 0.8 W/kg average SAR.

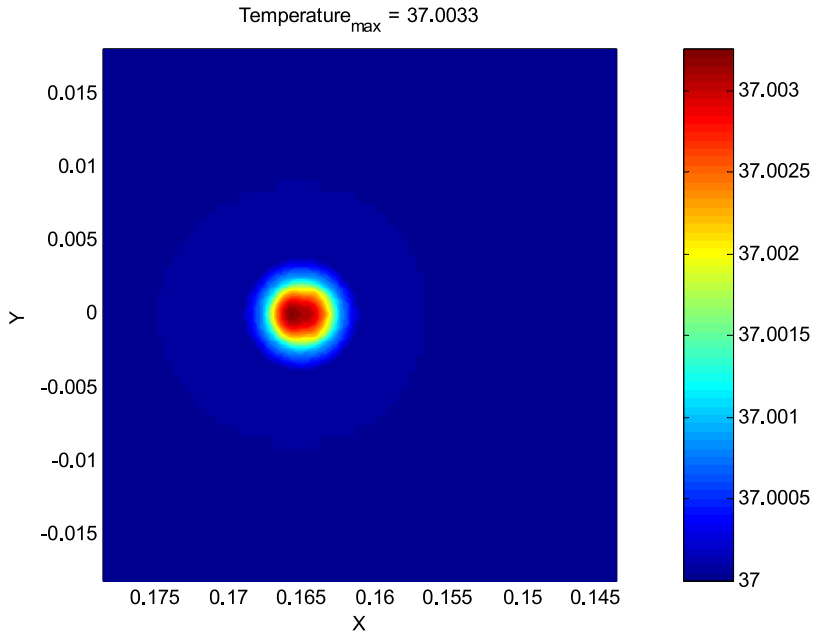

FIG. 8. Temperature distribution on the XY observation plane cutting the centre of the pineal gland in-vitro model (frequency=1800MHz).

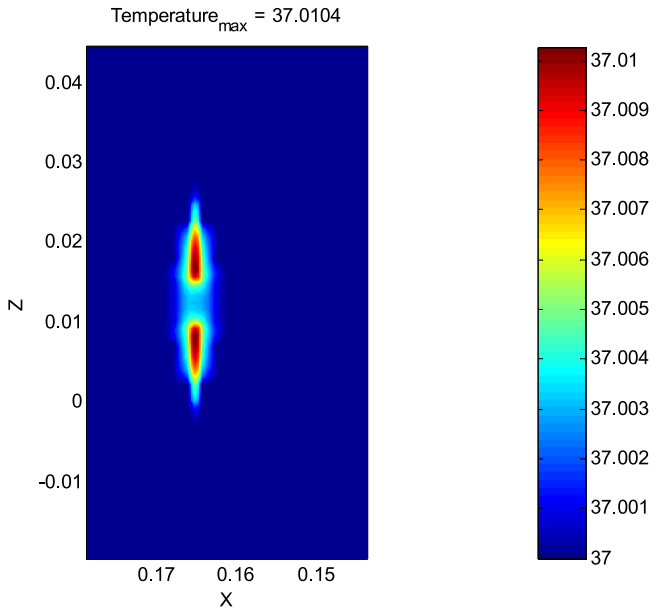

FIG. 9. Temperature distribution on the XZ observation plane cutting the centre of the pineal gland in-vitro model (frequency=1800MHz).

the computed temperature distributions on the XY, XZ, YZ observation planes, respectively. The observation planes are at the centre of the in-vitro model.

From Figure 8–10, we can find the maximum temperature rise in the biological sample is very small, these results exclude the possibility of thermally induced health hazards from cell phone radiofrequency radiation for a healthy person. The results agree with those of many other researchers. R Cooke *et al* show that use of mobile phones does not increase leukaemia risk;[9] T Takebayashi *et al.* observed no increase in overall risk of glioma or meningioma in relation to regular mobile

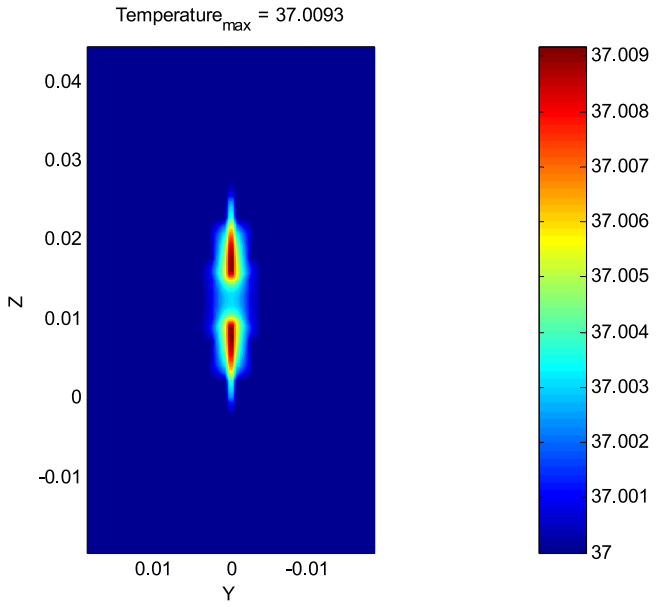

FIG. 10. Temperature distribution on the YZ observation plane cutting the centre of the pineal gland in-vitro model (frequency=1800MHz).

phone use;[10] The research by MJ Schoemaker suggests that there is no substantial risk of acoustic neuroma in the first decade after starting mobile phone use;[11] The result of F Malek et al. indicates that no negative health effect can be associated with electromagnetic field (EMF) exposure;[12] The study by C Johansen provides no support for an association between mobile phones and ocular.[13]

Byeon and Back discovered that melatonin level increased as temperature increased when rice seedlings were exposed to various temperatures for 1 hr.[14] Melatonin which is secreted by the pineal gland in the brain is a major regulator of core body temperature. Hence, temperature rise due to EM exposure may cause body's melatonin level to increase. Many experiments do show increased melatonin levels after exposure to magnetic or electromagnetic fields.[15–17] So hypothetically, the results of temperature rise in the pineal gland might indicate that melatonin could be a good mechanistic candidate to explain potentially deleterious or salubrious effects of cell phone RF radiation. Melatonin is used to treat insomnia. Cohen *et al* proposed the hypothesis that a decrease in melatonin levels might promote the development of breast cancer in humans.[18] Melatonin has also been reported to exert additional functions in other organs.[19–23]

IV. CONCLUSION

Simulation of temperature and electromagnetic field inside pineal gland cell was for the first time performed to illustrate effectiveness of the FVM method. The results exclude the possibility of thermally induced health hazards from cell phone radiofrequency exposure. In future study, we will apply the method implicitly[24] to 3D multi-material model with non-uniform grids.

ACKNOWLEDGMENTS

The paper was supported by the National Natural Science Foundation of China (61370185).

[1] International Agency for Research on Cancer (IARC), *Non-Ionizing Radiation, Part 2: Radiofrequency Electromagnetic Fields*, IARC Monogr Eval Carcinog Risk Hum (2013), 102.
[2] Report of Partial Findings from the National Toxicology Program Carcinogenesis Studies of Cell Phone Radiofrequency Radiation in Hsd: Sprague Dawley SD rats (Whole Body Exposures), bioRxiv preprint first posted online May. 26, 2016.
[3] P. J. Roache, *Computational Fluid Dynamics*, Hermosa Publishers, 1976.

[4] H. H. Pennes, "Analysis of tissue and arterial blood temperatures in the resting human forearm," J. Appl. Physiol. **1**, 93–122 (1948).
[5] W. Cen, R. Hoppe, Z. Q. Cai, Z. Yu, and N. Gu, "Accurate 3D multi-material EM-thermal modelling," AIP Advances **7**, 025214 (2017).
[6] R. D. Richtmyer and K. W. Morton, *Difference Methods for Initial Value Problems*, New York: Wiley, 1967, [second edition].
[7] N. Marcuvity, *Waveguide Handbook*, IEE ELECTROMAGNETIC WAVES SERIES 21.
[8] W. Cen and N. Gu, "Efficient solution on solving 3D Maxwell equations using stable semi-implicit splitting method," AIP Advances **6**, 055005 (2016).
[9] R. Cooke, S. Laing, and A. J. Swerdlow, "A case-control study of risk of leukaemia in relation to mobile phone use," British Journal of cancer **103**, 1729–1735 (2010).
[10] T. Takebayashi *et al*, "Mobile phone use, exposure to radiofrequency electromagnetic field, and brain tumour: A case-control study," British Journal of Cancer **98**, 652–659 (2008).
[11] M. J. Schoemaker *et al.*, "Mobile phone use and risk of acoustic neuroma: Results of the Interphone case-control study in five north European countries," British Journal of Cancer **93**, 842–848 (2005).
[12] F. Malek, K. A. Rani, H. A. Rahim, and M. H. Omar, "Effect of short-term mobile phone base station exposure on cognitive performance, body temperature, heart rate and blood pressure of Malaysians," Scientific Reports **5**, 13206 (2015).
[13] C. Johansen, J. D. Boice, Jr., J. K. McLaughlin, H. C. Christensen, and J. H. Olsen, Mobile phones and malignant menoma of the eye, British Journal of Cancer **86**, 348–349 (2002).
[14] Y. Byeon and K. Back, "Melatonin synthesis in rice seedlings in vivo is enhanced at high temperatures and under dark conditions due to increased serotonin N-acetyltransferase and N-acetylserotonin methyltransferase activities," Journal of Pineal Research **56**, 189–95 (2014).
[15] J. Bakos, N. Nagy, G. Thuroczy et al., "Urinary 6-sulphatoxymelatonin excretion is increased in rats after 24 hours of exposure to vertical 50 Hz, 100 microT magnetic field," Bioelectromagnetics **18**, 190–192 (1997).
[16] A. Lerchl, A. Zachmann, M. A. Ali et al., "The effects of pulsing magnetic fields on pineal melatonin synthesis in a teleost fish (brook trout, Salvelinus fontinalis)," Neurosci Lett **256**, 171–173 (1998).
[17] H. Lewy, O. Massot, and Y. Touitou, "Magnetic field (50 Hz) increases N-acetyltransferase, hydroxy-indole-O-methyltransferase activity and melatonin release through an indirect pathway," Int J Radiat Biol **79**, 431–435 (2003).
[18] M. Cohen, M. Lippman, and B. Chabner, "Role of pineal gland in aetiology and treatment of breast cancer," Lancet **2**, 814–816 (1978).
[19] Y. L. Tain *et al*, "Melatonin prevents increased asymmetric dimethylarginine in young rats with bile duct ligation," Journal of Pineal Research **48**, 212–221 (2010).
[20] M. Pan, Y. L. Song, J. M. Xu, and H. Z. Gan, "Melatonin ameliorates nonalcoholic fatty liver induced by high-fat diet in rats," Journal of Pineal Research **41**, 79–84 (2006).
[21] P. Subramanian, S. Mirunalini, S. R. Pandi-Perumal, I. Trakht, and D. P. Cardinali, "Melatonin treatment improves the antioxidant status and decreases lipid content in brain and liver of rats," Eur J Pharmacol **571**, 116–119 (2007).
[22] Y.-L. Tain *et al*, "Melatonin regulates L-arginine transport and NADPH oxidase in young rats with bile duct ligation: Role of protein kinase C," Pediatr Res **73**, 395–401 (2013).
[23] D. Thong-Ngam, S. Samuhasaneeto, O. Kulaputana, and N. Klaikeaw, "N-acetylcysteine attenuates oxidative stress and liver pathology in rats with non-alcoholic steatohepatitis," World J Gastroenterol **13**, 5127–5132 (2007).
[24] W. Cen, R. Hoppe, and N. Gu, "Fast and accurate determination of 3D temperature distribution using fraction-step semi-implicit method," AIP Advances **6**, 095305 (2016).